Numerical prediction of fiber orientation in injection molding

H. Henry de Frahan, V. Verleye, F. Dupret, M.J. Crochet
Unité de Mécanique Appliquée
Université Catholique de Louvain
2, Place du Levant, 1348 Louvain-la-Neuve, Belgium.

to appear in

POLYMER COMPOSITES

Abstract

We develop a numerical method for calculating fiber orientation in the mid-surface of a molded part of small thickness. Two-dimensional fiber orientation is predicted on the basis of either Jeffery's equation or a constitutive equation for the orientation tensor. The calculation is fully transient; it is performed on a time-dependent flow domain. The method is based on finite elements. Updated finite element meshes are generated at every instant of filling and allow one to perform an accurate calculation of the orientation even along the boundary of the flow domain. The method is applied to several examples in plane and three-dimensional geometries.

1. Introduction

The prediction of fiber orientation in injection molding is of prime importance in the design of filled polymer parts with desired mechanical properties. It is well-known that anisotropic mechanical properties are intimately related to fiber orientation. The numerical simulation of filling and fiber orientation is a very difficult problem for several reasons : i. the flow process is transient and generally non-isothermal; ii. although the Hele-Shaw approximation is usually valid for the flow calculation, the effect of the fountain flow near the moving flow front is such that fibers do not travel from the gate to their final position within a surface parallel to the mid-surface; iii. despite recent progress, the constitutive equations for fiber orientation in arbitrary flows require further progress.

In the absence of coupling between flow calculation and fiber orientation, wide use has been made of Jeffery's model [1], which is however based on a number of strong hypotheses. Jeffery's theory has been generalized (see e.g.[2]) to the calculation of an orientation tensor. It is assumed that fiber orientation is described by a statistical distribution; it is then possible to define a set of orientation tensors which are governed by constitutive equations. The use of a finite number of orientation tensors requires a closure approximation [2]. However, it is also possible to generate general constitutive equations for the orientation tensor along the well-established principles of continuum mechanics. Several models have also been made available for calculating flows coupled with fiber orientation, such as Ericksen's theory for liquid crystals [3], the Dinh-Armstrong theory of the integral type [4] or the differential model by Lispscomb et al. [5].

Coupled models have recently been used for simulating the flow of fiber filled polymers [5-7]. These papers clearly show that the coupled calculation is a difficult problem, and that such theories are presently limited to relatively low volume fractions. For the decoupled theory, early work by Givler, Crochet, Pipes [8] and by Givler [9] was based on the use of Jeffery's model in a general flow field; more recently, Advani and Tucker [10] calculated the evolution of the orientation tensor in a compression molding application.

The purpose of the present paper is to apply the decoupled method to the calculation of fiber orientation in injection molding, on the basis of Jeffery's equation as well as an orientation tensor equation. It is clearly understood that using the decoupled method for injection molding applications relies on a number of strong hypotheses which may unvalidate the procedure in practical applications. It is known indeed that the presence of

fibers may strongly modify the flow from Poiseuille to plug type. The absence of fiber-flow interaction implies dilute fiber suspensions while volume fractions up to 50 percent are typical in injection molding. Still, we wish to show how numerical methods can demonstrate the effect of available theories. We assume at the outset that the molded parts have a small thickness as compared to other characteristic dimenions and that their mid-surface can be approximated by a set of planar facets. We wish to base the orientation calculation on a fully transient velocity field in a deforming domain but, at the present stage, we do not take fountain flow into account. Thus, our calculation is presently limited to the orientation in a region which surrounds the mid-surface of the part. In the case of shear-thinning, the width of the central region is large with respect to the actual thickness. We also limit ourselves to isothermal situations, although the method used for calculating the flow [11,12] has been extended to non-isothermal situations [13,14]. The implementation of our method in a non-isothermal calculation would not pose any difficulty.

In section 2 we recall the basic equations of injection molding simulation and of decoupled fiber orientation. In section 3, we briefly recall the finite element method used for calculating the flow. In sections 4 and 5, we explain in some detail the numerical method which we have developed for either solving Jeffery's equation or for calculating the orientation tensor. In section 6, we test the convergence of the numerical method, and we also evaluate the influence of the initial conditions and of the closure approximation. Finally, we solve in section 7 two orientation problems on the basis of a complex geometry. In particular, we show that orientation distributions based on either Jeffery's equation or on an orientation equation give essentially the same results.

2. Basic equations

2.1. Injection molding

We wish to calculate the evolution of fiber orientation in the mid-surface of a thin molded part, in which the thickness is much smaller than other characteristic dimensions. We consider mid-surfaces without ribs or branchings. Under such conditions, it is possible to obtain a good approximation of the flow field with the use of the lubrication approximation, based on the fact that the velocity gradients in the thickness are much larger than the gradients in the mid-surface. One then obtains the Hele-Shaw approximation of the viscous flow [15], with the consequence that the velocity field can be derived from a potential. In the present paper, we limit ourselves to isothermal flow, although the method briefly described in section 3 has been extended to non-isothermal flow.

Let p denote the pressure at a point of the mid-surface. It can be shown that the average velocity $\bar{v}$ in the mold is given by the equation

$$\bar{v} = -\frac{\Sigma}{c} \nabla p \,, \tag{1}$$

where c is the half thickness of the mold and Σ is a scalar given by

$$\Sigma = \int_0^c \xi^2/\eta \; d\xi \,, \tag{2}$$

η is the shear viscosity at distance ξ from the mid-surface. From the conservation of mass, one finds that the pressure satisfies the following elliptic equation,

$$\nabla \cdot (\Sigma \nabla p) = 0 \,, \tag{3}$$

with boundary conditions of the Dirichlet type on the moving front, and of the Neumann type on the sides of the mold and at the gates, where the flow rate is imposed. In solving (3) with Σ defined by (2); we make the important hypothesis that the velocity field is decoupled from the fiber orientation in the fluid. In later work, it will be necessary to introduce an anisotropic behavior of the fluid caused by the preferred orientation of the fibers.

The flow front moves with velocity $\bar{v}$ in view of the mass conservation. However, for calculating the fiber orientation in the mid-surface, it is necessary to take into account the velocity field in that surface. Since the pressure does not vary throughout the thickness of the mold in the Hele-Shaw representation of the flow, we may use a fully developed Poiseuille velocity profile for predicting the mid-surface velocity on the basis of $\bar{v}$. For a power-law fluid with a power index n, one obtains

$$v = \bar{v} \; (2n+1)/(n+1) \,, \tag{4}$$

where v is the velocity vector in the mid-surface.

We will explain in section 3 how we calculate the velocity field in a mold of arbitrary shape made of a number of planar facets. The velocity field that we will refer to in fiber orientation equations is given by (4).

2.2. Fiber orientation : Jeffery's equation

A very simple model based on Jeffery's work [1] has been widely used over recent years for calculating the evolution of fiber orientation in viscous flows. Jeffery's equations are based on a number of strong hypotheses : one considers a single fiber of ellipsoidal shape in a Newtonian solvant, where the velocity gradient is uniform. However, experimental work [16] has shown the usefulness of Jeffery's equations, at least on a qualitative basis.

Let us represent a rigid fiber by means of a unit vector **p** with its origin at the centroid of the fiber which translates with the velocity of the fluid. Jeffery's equations state that the orientation of the fiber varies with time according to the following evolution equation,

$$\dot{p}_i = \omega_{ij}\, p_j + \lambda\, [d_{ij}\, p_j - d_{kl}\, p_k\, p_l\, p_i] \quad , \tag{5}$$

where

$$\omega_{ij} = \frac{1}{2}\left(\frac{\partial v_i}{\partial x_j} - \frac{\partial v_j}{\partial x_i}\right) \quad ,$$

$$d_{ij} = \frac{1}{2}\left(\frac{\partial v_i}{\partial x_j} + \frac{\partial v_j}{\partial x_i}\right) \quad , \tag{6}$$

and λ is a geometrical factor which vanishes for a spherical particle and takes the unit value for a very long fiber.

In the present work, we will be concerned with fiber orientation in planar facets, and we will assume that the fibers are contained in the facets. We may thus limit ourselves to the planar equivalent of (5). Let (x,y) denote a set of local Cartesian coordinates in the plane, (u,v) the velocity components, and ϕ the angle between the fiber and the x-axis. Equation (5) then becomes

$$\dot{\phi} = \frac{1}{2}\left(\frac{\partial v}{\partial x} - \frac{\partial u}{\partial y}\right) + \lambda\left[\frac{1}{2}\left(\frac{\partial v}{\partial x} + \frac{\partial u}{\partial y}\right)\cos 2\phi - \frac{1}{2}\left(\frac{\partial u}{\partial x} - \frac{\partial v}{\partial y}\right)\sin 2\phi\right] , \tag{7}$$

where $\dot{\phi}$ is the material derivative given by

$$\dot{\phi} = \partial\phi/\partial t + u\,\partial\phi/\partial x + v\,\partial\phi/\partial y \quad . \tag{8}$$

Eq.(7) allows us to calculate the variation of the angle ϕ for a single fiber moving in the mid-plane of the facet [8]. However, it is also possible to consider (7) as a partial differential equation for calculating an orientation field ϕ (x;y;t) [9]. Boundary conditions on ϕ are then imposed along a line crossing the characteristics. For injection molding applications, the fiber orientation field is imposed at the gates.

The selection of ϕ as an orientation variable is appropriate for calculating the evolution of the orientation of a fiber along its pathline. However, it is inappropriate for calculating fields in molds where flow fronts are meeting behind obstacles or in the case of multiple gates. Let us consider a simple example in Fig.1, where two flow fronts are meeting while they originate from different gates. The true orientation of a fiber is defined *modulo* π; two fibers with respective orientations ϕ and $\phi+m\pi$ (integer m) are in fact parallel. However, in a numerical calculation, we would obtain a discontinuity of the orientation field at the weldline. The problem of multiple definition of the orientation can be solved by selecting the variables $S=\sin 2\phi$ and $C=\cos 2\phi$ as representative of the fiber orientation. For the situation of Fig.1, C and S would always be continuous at the weldline when the fibers are parallel. On the basis of (7); it is easy to obtain partial differential equations governing the evolution of C and S, i.e.

$$\dot{C} = -S\left(\frac{\partial v}{\partial x} - \frac{\partial u}{\partial y}\right) - \lambda S\left[\left(\frac{\partial v}{\partial x} + \frac{\partial u}{\partial y}\right) C - \left(\frac{\partial u}{\partial x} - \frac{\partial v}{\partial y}\right) S\right] \quad ,$$

$$\dot{S} = C\left(\frac{\partial v}{\partial x} - \frac{\partial u}{\partial y}\right) + \lambda C\left[\left(\frac{\partial v}{\partial x} + \frac{\partial u}{\partial y}\right) C - \left(\frac{\partial u}{\partial x} - \frac{\partial v}{\partial y}\right) S\right] \quad . \tag{9}$$

Compatible values for C and S are imposed along a line crossing the characteristics. We will explain in section 4 the numerical method which has been developed for integrating (9) on an evolving flow domain.

2.3. Fiber orientation : orientation tensor

Apart from a number of inherent hypotheses, a difficulty with the use of Jeffery's equation is that it does not predict the anisotropy of fiber orientation, unless one assigns a number of different orientations along the inlet boundary [8]. The full information on anisotropy would be given by a probability distribution function which, in planar flow, would consist of a function $\Psi(\phi)$; for a given material point, the product $\Psi(\phi)\, d\phi$ gives the probability of finding a fiber with an orientation between ϕ and $\phi+d\phi$. The calculation of the function $\Psi(\phi)$ itself throughout a flow domain is a formidable task; rather, one resorts to the calculation of orientation tensors [2]. The second- and fourth-order orientation tensors are, for example, defined by

$$\alpha_{ij} = \int_0^{2\pi} \Psi(\phi) p_i p_j \, d\phi,$$

$$\alpha_{ijkl} = \int_0^{2\pi} \Psi(\phi) p_i p_j p_k p_l \, d\phi \,, \qquad (10)$$

where p_i is the i-th component of $\mathbf{p}$.

On the basis of the continuity condition for the distribution function and an equation of state for the evolution of fiber orientation, it is in principle possible to obtain an equation describing the change of orientation tensors. If one uses for example Jeffery's equation, one finds that [2]

$$\dot{\alpha}_{ij} = \omega_{ik}\, \alpha_{kj} - \alpha_{ik}\, \omega_{kj} + \lambda(d_{ik}\, \alpha_{kj} + \alpha_{ik}\, d_{kj} - 2\alpha_{ijkl}\, d_{kl}) \,. \qquad (11)$$

The evolution equation for the second-order orientation tensor involves the fourth-order one, while the evolution equation for the latter would involve the sixth-order tensor. It is thus necessary to introduce a closure approximation if one wishes to calculate the distribution of α_{ij} on the basis of a velocity field. In what follows, we will primarily use the simplest closure approximation, i.e.

$$\alpha_{ijkl} = \alpha_{ij}\, \alpha_{kl}. \qquad (12)$$

Further discussion on the closure approximation may be found in [2,17].

The hypotheses underlying Eq.(11) are the same as those of Jeffery's equation, since the latter has been used for obtaining (11). The first advantage of (11) is that it provides an estimate of the orientation distribution instead of the orientation of a single fiber. The second is that (11) has the form of an invariant equation of state which lays the background for further development. Indeed, (11) and (12) may be written in the more general tensor form

$$\overset{0}{\underline{\alpha}} = \underline{A}(\underline{\alpha}, \underline{d}) \ , \tag{13}$$

where $\overset{0}{\underline{\alpha}}$ is the corotational derivative of $\underline{\alpha}$ defined by

$$\overset{0}{\underline{\alpha}} = \dot{\underline{\alpha}} - \underline{\omega}\,\underline{\alpha} + \underline{\alpha}\,\underline{\omega} \ , \tag{14}$$

and $\underline{A}$ is a tensor function of $\underline{\alpha}$ and $\underline{d}$. Eq.(13) is invariant upon rigid body motions. With (11) and (12); the tensor function $\underline{A}$ is given by

$$\underline{A}\,(\underline{\alpha}, \underline{d}) = \lambda[\underline{d}\,\underline{\alpha} + \underline{\alpha}\,\underline{d} - 2\mathrm{tr}(\underline{\alpha}\,\underline{d})\,\underline{\alpha}] \ . \tag{15}$$

It is clear however that other tensor functions can be introduced for calculating the orientation tensor. Typically, on the basis of Folgar and Tucker's work [18], one obtains an additional term for $\underline{A}(\underline{\alpha},\underline{d})$ which is also invariant upon rigid body motions. The continuum mechanics approach of the evolution equation for the orientation tensor gives more freedom with respect to the strong hypotheses (i.e. a single fiber in a Newtonian fluid) underlying Jeffery's equation.

We note that Eq.(11) is hyperbolic; it requires an initial distribution in the flow domain together with boundary conditions on a line crossing the characteristics of the first order system (9); i.e. at the gates. For injection molding applications, we would for example impose an isotropic fiber distribution at the gates.

3. Flow calculation

We wish to calculate fiber orientation over a domain which is evolving with time. Fig.2a shows a typical planar problem : a rectangular plate is injected through a central gate

and two lateral ones. Fig.2a shows the successive flow fronts during the filling of the part. In the early stage of the filling, we need to consider three separate flow domains which later form two and then a single flow domain after junction of the various fronts. In order to calculate fiber orientation as a function of time, we need to cover the flow domain at every time t with a finite element mesh. Let us briefly review the method which has been developed on the basis of a pre-selected finite element mesh [11,12].

The flow domain of Fig.2a is covered by a finite element mesh of either quadrilateral or triangular elements shown in Fig.2b. The time is discretized in terms of a number of finite intervals; let t_n denote an intermediate time at which we describe the iterative procedure. At time t_n, let us consider in Fig.2c the boundary of the flow domain which presently consists of two separate closed curves. Such boundaries allow us to separate the finite elements of the initial mesh into three classes : i. the elements behind the flow front which are fully filled with fluid; ii. the elements outside the flow domain which are empty; iii. the elements which are partially filled.

Our procedure consists of first preserving the elements of the first class which cover most of the flow domain, thus ensuring without difficulty a well designed mesh. Next, we need to draw a finite element mesh in the region lying between the flow front and the filled elements. For that region, we use a fully automatic mesh generator which links existing nodes with those identifying the flow front. The final mesh generated for the situation of Fig.2c is shown in Fig.2d. The procedure is valid for flat as well as three-dimensional surfaces; several examples will be shown in later sections. Despite its apparent simplicity, the automatic generation of finite element meshes at every time step requires a very complex algorithm if one wishes to generate meshes for the filling of molds of arbitrary geometry and with an arbitrary gate distribution. A detailed description of the algorithm is available in [19].

Let Ω_n denote the flow domain at time t_n, and let Ω_n^h denote the corresponding finite element mesh. In the present paper, we limit ourselves to isothermal flow, although the method has been extended to non-isothermal flow [13]. The primitive variable is the pressure, with nodal values P_i^n at the nodes of Ω_n^h. The discretized system for calculating the P_i^n's is obtained by applying Galerkin's method to (3) (see e.g.[13] or [15]). For a Newtonian fluid, the discretized system is linear while an iterative procedure is necessary for generalized Newtonian flow. We use for the pressure a P^2-C^0 representation.

On the basis of (1) and (4); it is then possible to calculate the velocity field in the mid-surface within Ω_n^h which is however discontinuous at element boundaries. Along the flow front, a continuous representation of the velocity field is obtained by means of a consistent method. Such a continuous representation is required for calculating the motion of the boundary from time t_n to $t_{n+1} = t_n + \Delta t$, and for defining the domain Ω_{n+1}^h.

In later sections, we will assume that we have calculated a sequence of finite element meshes Ω_n^h on which we know the discretized pressure field and the corresponding (discontinuous) velocity field. For three-dimensional domains, described by a set of plane facets, Ω_n^h consists of a set of plane meshes, with compatible finite element distributions along the edges. In Fig.3a we show a set of boundary lines on a wind-breaker described by a three-dimensional surface. Fig.3b shows the initial mesh covering the whole domain while Fig.3c shows an intermediate mesh.

4. Numerical integration of Jeffery's equation

4.1. Method of weighted residuals

Let us now return to Eq.(9) which we wish to integrate over a flow domain which is evolving with time, as described in section 3. The primitive variables for describing the orientation are the functions C and S which are represented by means of a P^1-C^0 interpolation over Ω_n^h, i.e.

$$C = \Sigma\, \psi_i\, C_i\,(t) \quad , \qquad (16)$$

$$S = \Sigma\, \psi_i\, S_i\,(t) \quad ,$$

where C_i, S_i are nodal values which depend upon time while the ψ_i's are shape functions. In order to transform the system (9) into a set of ordinary differential equations, we first apply the method of weighted residuals; for a set of weighting functions W_i we write

$$\int_{\Omega_n^h} W_i \left\{ \frac{\partial C}{\partial t} + \frac{\partial C}{\partial x} u + \frac{\partial C}{\partial y} v + S \left(\frac{\partial v}{\partial x} - \frac{\partial u}{\partial y} \right) \right. \qquad (17)$$

$$+\lambda S\left[\left(\frac{\partial v}{\partial x}+\frac{\partial u}{\partial y}\right) C-\left(\frac{\partial u}{\partial x}-\frac{\partial v}{\partial y}\right) S\right]\Big\} \, d\Omega = 0 \ ,$$

while a similar integration is performed on the second equation (9).

The structure of Eq.(17) results in a difficulty which is inherent to the flow calculation of section 3. We have shown that the velocity field is calculated from the pressure which has a continuous finite element representation. The calculated velocity field is therefore discontinuous, and its first derivatives appearing in (17) do not exist. A way of solving the problem is to calculate on Ω_n^h a smoothed velocity field by means of a least square procedure which would however be very expensive, since it requires the solution of two large linear systems at every time step. A cheaper and easy approach is to perform an integration by parts on every term containing velocity gradients, and to calculate the resulting boundary integrals. Typically we have

$$\int_{\Omega_n^h} W_i S C \frac{\partial v}{\partial x} \, d\Omega = \int_{\Omega_n^h} \left[\frac{\partial}{\partial x}(W_i S C v) - v \frac{\partial}{\partial x}(W_i S C)\right] d\Omega$$

$$= -\int_{\Omega_n^h} v \frac{\partial}{\partial x}(W_i S C) \, d\Omega + \int_{\partial\Omega_n^h} n_x v W_i S C \, d\partial\Omega. \qquad (18)$$

In order to select an appropriate weighting function for integrating (18); it is interesting to consider a very simple problem schematized in Fig.4. In a rectangular plate filled with fluid, we consider a vertical uniform velocity field. In the initial configuration, we consider a uniform orientation field with $\phi=\pi/4$. However we modify the orientation in the entry section, and impose a value of $-\pi/4$. The exact solution of the problem would show the motion of the discontinuity with the uniform velocity of the fluid. The discretized solution is of course unable to predict a discontinuous field, which is necessarily smoothed. Applying Galerkin's formulation, we select weighting functions W_i identical to the shape functions ψ_i in (16). The orientation as a function of coordinate y for various instants is shown in Fig.5a. We find the expected result that Galerkin's method applied to a hyperbolic

problem generates spatial oscillations in the presence of high gradients. We thus resort to an upwinding scheme. The streamline-upwind Petrov-Galerkin (SUPG) scheme [20] would be ideal if the velocity field were continuous. However, the discontinuous nature of the discretized velocity field forces us to calculate derivatives of the weighting functions W_i; we are thus not allowed to introduce discontinuous weighting functions which are proper to the SUPG scheme. We resort to a non-consistent streamline-upwind (SU) scheme, in which the modified weighting function is only applied to the advective terms in (9). The evolving orientation field based on SU is shown in Fig.5b, where we find that the wiggles of Fig.5a have disappeared, although artificial smoothing has been introduced in the solution. For technical details on the application of streamline-upwinding, the reader is referred to [20].

4.2. Time integration

Let us assume that, at time t_n, we know the orientation represented by C_n and S_n over the domain Ω_n^h. The steps of the time integration are as follows :

i. On the basis of the discretized pressure field P_n on Ω_n^h, calculate on Ω_n^h a provisional orientation field at time $t_{n+1} = t_n + \Delta t$, denoted by C* and S*.
ii. Similarly, on the basis of P_n, calculate the new flow front and create Ω_{n+1}^h by means of the remeshing technique explained in section 3.
iii. Interpolate or extrapolate the orientation field C*, S* from Ω_n^h to Ω_{n+1}^h, in order to obtain C_{n+1} and S_{n+1}.
iv. Calculate a new pressure field P_{n+1} on Ω_{n+1}^h.

For calculating C* and S*, we use the fourth order Runge-Kutta algorithm. The selection of the time step is based on Courant's criterion

$$\Delta t < h/|v| \quad , \tag{19}$$

where h represents the size of an element and $|v|$ the norm of the velocity.

Let us explain in some detail the calculation of C_{n+1} and S_{n+1} over Ω_{n+1}^h. Fig.6a shows the superposition of Ω_n^h and Ω_{n+1}^h. We start with the calculation of an intermediate orientation field C* and S* over Ω_n^h; next, we need to evaluate C_{n+1} and S_{n+1} on Ω_{n+1}^h on

the basis of C* and S*. The finite element meshes Ω^h_n and Ω^h_{n+1} may differ in two respects : i. Ω^h_{n+1} covers in general a domain larger than Ω^h_n; ii. even on the common region, the finite elements may be different in view of the remeshing procedure. The adopted procedure consists of evaluating C_{n+1} and S_{n+1} by means of a least square criterion, i.e. the minimization of the integral

$$I = \int_{\Omega^h_{n+1}} (C_{n+1} - C^*)^2 \, d\Omega \tag{20}$$

and a similar expression for S. In view of (16); the minimum of I in (20) is obtained when, for node i, we have

$$\int_{\Omega^h_{n+1}} \psi_i \, C_{n+1} \, d\Omega = \int_{\Omega^h_{n+1}} \psi_i \, C^* \, d\Omega \quad . \tag{21}$$

The evaluation of the left-hand side in (21) follows a standard procedure. The integral on the right hand side is calculated by means of a numerical quadrature over the elements of Ω^h_{n+1}. Let ω_{n+1} be such an element; we write

$$\int_{\omega_{n+1}} \psi_i \, C^* \, d\Omega = \sum_k \psi_i (x_k) \; C^*(x_k) \, \zeta_k \, , \tag{22}$$

where x_k refers to the numerical integration point and ζ_k is the corresponding weight. There are now two possibilities :

i. $x_k \in \Omega^h_n$. The value of $C^*(x_k)$ may then be easily calculated.

ii. $x_k \notin \Omega^h_n$. The value of $C^*(x_k)$ is then calculated by means of an analytical continuation. The procedure is schematized in Fig.6a. One calculates the normal from x_k to the boundary of Ω^h_n. Let x^* denote the intersection between the normal and Ω^h_n, we write

$$C^*(\mathbf{x}_k) = C^*(\mathbf{x}^*) + \nabla C^*(\mathbf{x}^*) \cdot (\mathbf{x}_k - \mathbf{x}^*) \ . \qquad (23)$$

A similar procedure applies for calculating S*.

There are circumstances, as shown in Fig.6b, where $\mathbf{x}_k$ corresponds to more than one point on the boundary of Ω_n^h; it is the case in particular when two or more flow fronts meet for forming a weldline. The value of $C^*(\mathbf{x}_k)$ is then calculated by an averaging procedure. The averaging between moving flow fronts is precisely the reason why we need to represent the orientation by means of C and S; if we were using the orientation angle ϕ, an interpolation between ϕ and $(\phi+\pi)$ would give us a value of $\phi+\pi/2$, although the fibers have the same orientation on both fronts.

4.3. Flow around folds

A difficult problem occurs when the flow front crosses a fold between planar facets. When the length of the fibers is larger than the thickness of the mold, it is clear that the fold would have a dominant effect on the orientation of a fiber. We assume that the fibers are short enough so that their orientation with respect to the direction of the edge is preserved when the flow front passes the fold. Typically, let us consider in Fig.7 a rectangular plate injected from one end and a plate of the same size bent in four planar facets. The assumption is that the final state of orientation in the bent plate is the same as in the flat plate. Let ϕ denote the orientation in a facet with coordinates x,y, while ϕ',x',y' are the corresponding quantities in an adjacent facet (Fig.8). Let α denote the angle between 0'x' and 0x. Across the fold, we impose

$$\phi = \phi' + \alpha. \qquad (24)$$

4.4. Anisotropic state of orientation

One of the objectives of the numerical simulation is to predict the anisotropy of the mechanical properties of the molded part in view of a preferred fiber orientation. In order to achieve that goal, we solve several problems with different orientations at the gates. In most examples, we found that all fibers would soon align in essentially the same orientation.

In a given Cartesian coordinate system, it is easy to calculate an orientation tensor on the basis of the quantities C and S. Indeed, the x- and y- components of $\mathbf{p}$ are $\cos\phi$ and $\sin\phi$; in view of the definition (10) we have

$$\alpha_{11} = < \cos^2\phi > = \frac{1}{2}(1 + < C >) ,$$
$$\alpha_{22} = 1 - \alpha_{11} , \qquad (25)$$
$$\alpha_{12} = < \cos\phi \sin\phi > = \frac{1}{2} < S > ,$$

where the brackets denote the average. Calculating the fields C and S on the basis of several initial orientations, we may thus obtain an estimate of α_{ij} through an averaging process.

5. Numerical calculation of the orientation tensor

In the present section, we wish to explain the numerical integration of (5) over a moving domain during injection molding. Many of the features of the algorithm are similar to those of section 4; we will thus necessarily be brief.

5.1. Method of weighted residuals

We wish to calculate the orientation tensor α_{ij} defined by (10) while the evolution equation is given by (11). We know at the outset that α_{ij} is symmetric, has a unit trace and is positive definite. Its eigenvalues λ are such that $0 \le \lambda \le 1$. The primitive variables for describing the orientation are the functions α_{11} and α_{12} which are represented by means of a P^1-C^0 interpolation over Ω_n^h, i.e.

$$\alpha_{11} = \Sigma \psi_i \ \alpha_{11}^i (t) ,$$
$$\alpha_{12} = \Sigma \psi_i \ \alpha_{12}^i (t) . \qquad (26)$$

In order to obtain ordinary differential equations in terms of α_{11}^i (t) and α_{12}^i (t); we apply the method of weighted residuals, as in (17), to the orientation equation (11). In order to easily consider various types of closure approximations, we introduce them at the discrete level. More precisely, we select for α_{ijkl} a representation of the type

$$\alpha_{ijkl} = \Sigma \ \psi_m \alpha_{ijkl}^m , \qquad (27)$$

the nodal values of α_{ijkl} are thus related to the nodal values of α_{ij}. The quadratic closure approximation (12) then becomes

$$\alpha_{ijkl} = \Sigma\, \psi_m \alpha^m_{ij}\, \alpha^m_{kl} \qquad (28)$$

instead of

$$\alpha_{ijkl} = (\Sigma\, \psi_m\, \alpha^m_{ij})\ (\Sigma\, \psi_n\, \alpha^n_{kl}) \ . \qquad (29)$$

Both versions have the same nodal values and converge when the size of the elements decreases.

The problems encountered in section 4.1 with the derivatives of the velocity field and the need for an upwinding scheme are similar when one calculates the orientation tensor; we perform again an integration by parts and apply a streamline upwinding technique.

5.2. Time integration

The time integration described in section 4.2 applies to the calculation of α_{ij}. In particular, we use a fourth-order Runge-Kutta algorithm for calculating the orientation α^*_{ij} at time t_{n+1} on Ω^h_n. An analytic continuation is also used for extrapolating the orientation from Ω^h_n to $\Omega^{\ h}_{n+1}$.

5.3. Flow around folds

When the flow front crosses a fold, we apply the same ideas as in section 4.3. Returning to Fig.8, let β_{ij} denote the matrix of director cosines of the (x',y') axes with respect to (x,y). Let α_{ij}, α'_{ij} denote the orientation tensor on both sides of the edge. The continuity condition states that, at the edge,

$$\alpha'_{ij} = \beta_{ik}\, \beta_{jl}\, \alpha_{kl} \ . \qquad (30)$$

5.4. Stability control

It is found that, in many flows, the anisotropy becomes highly pronounced, with one of the eigenvalues of the orientation tensor being very close to one. In the extrapolation procedure from Ω^h_n to $\Omega^{\ h}_{n+1}$ as described in section 4.2, it may happen that one of the eigenvalues becomes larger than one; such a process is often followed by an instability of the

numerical scheme. It is then necessary to adjust the extrapolated matrix in order to preserve its unit trace and its positiveness while maintaining the eigenvectors of the orientation tensor.

Let α^*_{ij} denote the extrapolated orientation tensor, which has an eigenvalue $(1+\varepsilon)$ while the other is $(-\varepsilon)$. We substitute for α^*_{ij} a tensor α_{ij} defined as follows,

$$\alpha_{ij} = \gamma \alpha^*_{ij} + \beta \delta_{ij} \quad , \tag{31}$$

where γ and β are scalars and δ_{ij} is the unit tensor. The preservation of a unit trace imposes that

$$\gamma + 2\beta = 1 \quad . \tag{32}$$

The eigenvalues Λ of α_{ij} are related to those of α^*_{ij} by

$$\Lambda = \beta + \gamma\Lambda^* \quad . \tag{33}$$

When an eigenvalue of α^*_{ij} equals $(-\varepsilon) < 0$, we obtain an admissible tensor α_{ij} by selecting

$$\gamma = (1 + 2\,\varepsilon)^{-1} \quad , \qquad \beta = \varepsilon(1+2\varepsilon)^{-1} \quad . \tag{34}$$

A control of the size of the eigenvalues is systematically applied after every extrapolation from Ω^h_n to Ω^h_{n+1}.

In order to show the anisotropy of the fiber orientation field, we calculate the eigenvectors of α_{ij} and plot their size and orientation over the flow domain.

6. Numerical tests

We have shown in sections 4 and 5 that the numerical methods used for calculating either a fiber orientation based on Jeffery's equation or an orientation tensor are essentially the same. In the present section, we wish to analyze a number of features based on the prediction of the orientation tensor. In section 7, we will compare results obtained with both approaches. We have assumed in all the examples below that the fluid is Newtonian and isothermal.

6.1. Convergence test

Let us return to the problem of Fig.2. We assume that, at the gates, we inject fibers with an isotropic orientation, i.e. $\alpha_{11} = \alpha_{22} = 0.5$, $\alpha_{12} = 0$. The aspect ratio of the fibers is 2; we select on purpose a low value in order to delay the development of the anisotropic orientation. We have performed the calculations on three finite element meshes which contain respectively 276, 622 and 1462 elements. They are shown in Fig.9; we find that the size h of an element has been respectively divided by 2 and by 4. The succesive flow fronts have been shown in Fig.2a. Fig.10 shows the map of the eigenvectors of the orientation tensor over the whole domain with the coarsest and the finest mesh. The correspondence is obviously good; we note in particular the changes of orientation which occur at the weldlines due to the separate gates. For a quantitative comparison, we show in Fig.9 a horizontal and a vertical cross-section along which we evaluate the components α_{11} and α_{12} of the orientation tensor. The results are shown in Fig.11. We find some difference between the first and the second mesh on the horizontal cross-section, while the second and the third mesh give essentially the same results. Differences may be found in the upper right corner where the finest mesh allows for a precise calculation of the velocity field at the last filling stage. The results obtained on the vertical cross-section are essentially the same.

6.2. Dependence on initial conditions

In Fig.12, we show a finite element mesh (a) and the successive flow fronts (b) for the filling of a podium with a square hole. We have calculated the orientation tensor with an aspect ratio of 200 with two different orientations at the gates. In Fig.12c, the eigenvalues are equal at the gate and correspond to an isotropic distribution. In Fig.12d, the fibers are all oriented in the same direction. The plots of the eigenvectors show that it takes a very short distance for the fibers in both cases to align in the same direction; the initial state of orientation has little impact upon the final configuration.

6.3. Closure approximation

In the results shown above, we have used the quadratic closure approximation given by (12). There are other types of closure approximations; for example, the linear closure approximation given in [2] is better for a completely random distribution of orientation, while the quadratic one is exact for a uniaxial alignment. A hybrid closure approximation given in [2] mixes the quadratic and linear closures for covering a wider range of orientation

states. In Fig.13, we show the finite element mesh covering a mold (a); the successive flow fronts (b); and the orientation obtained with the quadratic closure (c) and an aspect ratio of 2. The orientation state obtained with the hybrid closure is essentially similar. For a quantitative comparison, we have drawn in Fig.13d a straight line crossing the flow domain. In fig.14, we plot the value of α_{11} as a function of an abscissa along that line for both closures. We find that the resulting orientation is the same except in a small region where the fibers are reorienting near the weldline. In our injection molding applications, the type of closure approximation seems to have little impact over the final state of orientation. This is due to the fact that the orientation alignment (due to the use of Jeffery's model) is high in the present geometrical configurations.

7. Examples

In the present section, we show two examples together with a comparison between Jeffery's orientation and the orientation tensor, with the same aspect ratio.

7.1. Filling of a dashboard

In Fig.15, we show the finite element mesh (a) and the flow fronts (b) for a part with four holes and two gates. The filling is characterized by several weldlines appearing behind the obstacles and at the junction of the flows coming from the separate gates. We have filled the mold with fibers of an aspect ratio of 2. Fig.16a shows the eigenvectors of the orientation tensor obtained on the basis of (11); while Fig.16b shows the average orientation of fibers based on Jeffery's equation with three different initial orientations. We expect both orientation tensors to be the same provided enough discrete initial orientations are considered at the outset. It is interesting to observe that in the present problem the orientation states obtained with both approaches are essentially similar, although we have only used three initial orientations for Jeffery's law. One should note the complex state of orientation along the weldlines behind the obstacles.

7.2. Filling of a windbreaker

In order to show a three-dimensional example, we return to the wind-breaker of Fig.3 on which we have again calculated the fiber orientation with both approaches. Fig.17a shows the eigenvalues of the orientation tensor with an aspect ratio of 100, while Fig.17b shows the corresponding figure with Jeffery's equation. Again, the results are essentially the same despite the small number of initial orientations.

It is found that the fibers are quickly aligned in the extensional direction of the flow, i.e. along the flow fronts, and that the edges do not modify the orientation, as expected from the hypotheses of sections 4.3 and 5.3.

8. Conclusions

We have shown that the calculation of fiber orientation, both by means of Jeffery's equation and an orientation tensor, can be coupled with the time-dependent calculation of injection molding, in plane and spatial geometries. Both approaches give essentially the same results with only three initial orientations for Jeffery's equation. We have shown that the final state of orientation shows little dependence upon the orientation at the gate . Although we have on purpose limited our developments to a Newtonian filling of the mold, the method is applicable as well to generalized Newtonian fluids although the validity of the orientation law may need to be modified. In theory, the validity of the present calculations is limited to dilute fiber solutions. High volume fractions would require a modified orientation law while the effect of volume fraction on velocity profile in the mold should be taken into account. Still, the present approach is helpful for a better understanding of fiber orientation together with a qualitative prediction of the orientation state.

Acknowledgements

The work of H. Henry de Frahan was supported by Owens Corning Fiber Glass (Belgium) and by a grant from IRSIA. The work of V. Verleye was supported in part by a grant from the SPPS (Service de programmation de la Politique Scientifique) and a collaboration with PSA in France.

References

[1] G.B. Jeffery, Proc. Roy. Soc., A102, 161 (1922).

[2] S.G. Advani, Ch. L. Tucker III, J. of Rheology, 31, 751 (1987).

[3] J.L. Ericksen, Arch. Rat. Mech. Anal., 4, 231 (1960).

[4] S.M. Dinh, R.C. Armstrong, J. Rheol., 28, 207 (1984).

[5] G.G. Lipscomb, M.M. Denn, D.V. Hur, D.V. Boger, J. Non-Newt. Fluid Mech., 26, 297 (1988).

[6] Y. Rosenberg, M.M. Denn, R. Keunings, J. Non-Newt. Fluid Mech., 37, 317 (1990).

[7] T.C. Papanastasiou, A.N. Alexandrou, J. Non-Newt. Fluid Mech., 25, 313 (1987).

[8] R.C. Givler, M.J. Crochet, R.B. Pipes, J. of Composite Materials, 17 , 330 (1983).

[9] R.C. Givler, in *Transport Phenomena in Material Processing*, Ed. M.M. Chen, J. Mazumdar, C.L. Tucker, ASME, New York, 99 (1983).

[10] S.G. Advani, Ch. L. Tucker III, A numerical simulation of short fiber orientation in compression molding, Polymer Composites, (1990).

[11] A. Couniot, M.J. Crochet, NUMIFORM 86, Ballkema, Mattiasson et al (eds); 165 (1986).

[12] A. Couniot, L. Dheur, O. Hansen, F. Dupret, NUMIFORM 89, Thompson et al (eds); Balkema, 235 (1989).

[13] F. Dupret, L. Vanderschuren, AICh E Jl.34, 12 (1989).

[14] F. Dupret, L. Dheur, Modeling and numerical simulation of heat transfer during the filling stage of injection molding, Proceedings of the Oji International Seminar on Advanced Heat Transfer in Manufacturing and Processing of New Materials, Tomakomai City, Hokkaido, Japan, October 1990.

[15] C.A. Hieber, S.F. Shen, J. Non-Newt. Fluid Mech., 7, 1, 1980.

[16] S.G. Mason, R. St Manley, Proc. Royal Society, Series A, 238, 117 (1957).

[17] S.G. Advani, Ch.L. Tucker III, J. of Rheology, 34, 367, 1990.

[18] F. Folgar, Ch. L. Tucker III, J. of Reinforced Plastics and Composites, 3, 98, 1984.

[19] A. Couniot, Ph. D. Thesis, Louvain-la-Neuve, 1991.

[20] A.N. Brooks, T.J.R. Hughes, Comput. Meth. Appl. Mech. Eng., 32, 199 (1982).

Captions for figures

Fig.1. Formation of a weldline in a flow originating from two distinct gates.

Fig.2. a. Successive flow fronts for the filling of a rectangular part through two lateral gates and a central one; b. initial finite element mesh; c. definition of the flow domain; d. finite element mesh covering the flow domain.

Fig.3. a. Successive flow fronts for the filling of a wind-breaker; b. initial finite element mesh; c. intermediate finite element mesh.

Fig.4. Uniform flow through a rectangular domain. A discontinuity in fiber orientation is propagated from the entry to the exit section.

Fig.5. Fiber orientation at various values of time along the vertical line AB in Fig.4; a. Galerkin method; b. Streamline-upwind method.

Fig.6. Extrapolation technique for calculating fiber orientation at time t_{n+1}; a. single flow front; b. two flow fronts move for forming a weldline.

Fig.7. Flow in a plane mold and in a folded mold.

Fig.8. Calculation of the change of orientation across folds.

Fig.9. Three finite element meshes for the problem of Fig.2 containing respectively a. 276 elements, b. 622 elements, c. 1462 elements.

Fig.10. Eigenvectors of the orientation tensor based on mesh a and mesh c of Fig.9.

Fig.11. Components α_{11} and α_{12} of the orientation tensor plotted along the lines AB and CD shown in Fig.9 for finite element meshes a(—); b(---) and c (- — • —).

Fig.12. Filling of a podium with a square hole : a. initial finite element mesh; b. successive flow fronts; c.d, fiber orientations corresponding to different initial conditions.

Fig.13. a. Initial finite element mesh; b. successive flow fronts; c. eigenvectors of the orientation tensor; c. cross section used in Fig.14.

Fig.14. Orientation component α_{11} along the cross-section of Fig.13 for the quadratic closure (—) and the hybrid closure (- — • —).

Fig.15. Filling of a dashboard with two gates : a. finite element mesh; b. successive flow fronts.

Fig.16. Fiber orientation distribution corresponding to the orientation tensor calculation (a) and Jeffery's law with three initial directions (b).

Fig.17. Fiber orientation in the wind-breaker of Fig.3 corresponding to the orientation tensor calculation (a) and Jeffery's law (b).

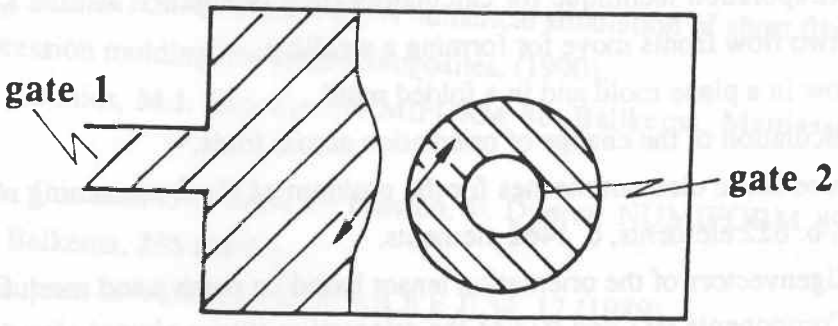

Fig.1. Formation of a weldline in a flow originating from two distinct gates.

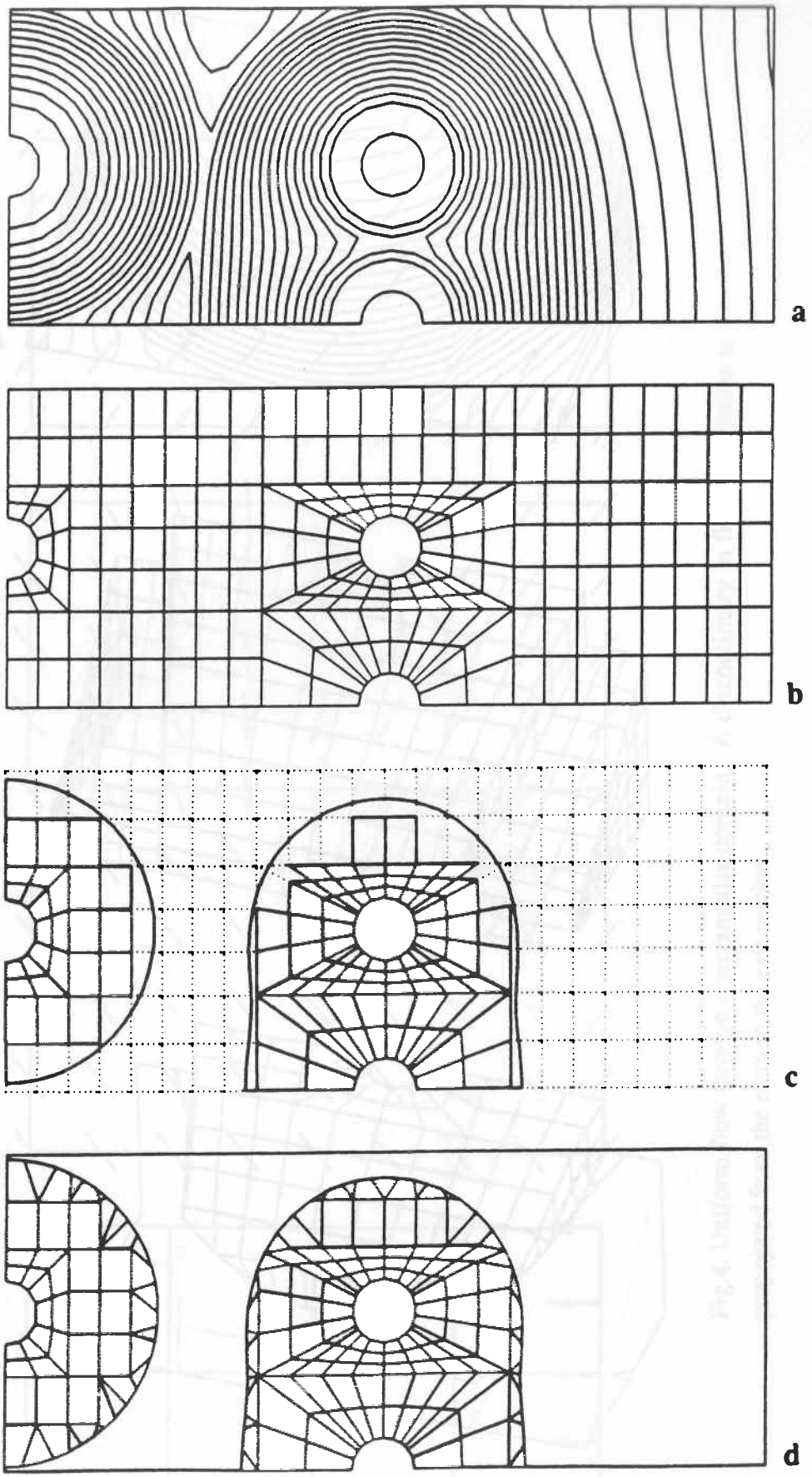

Fig.2. a. Successive flow fronts for the filling of a rectangular part through two lateral gates and a central one; b. initial finite element mesh; c. definition of the flow domain; d. finite element mesh covering the flow domain.

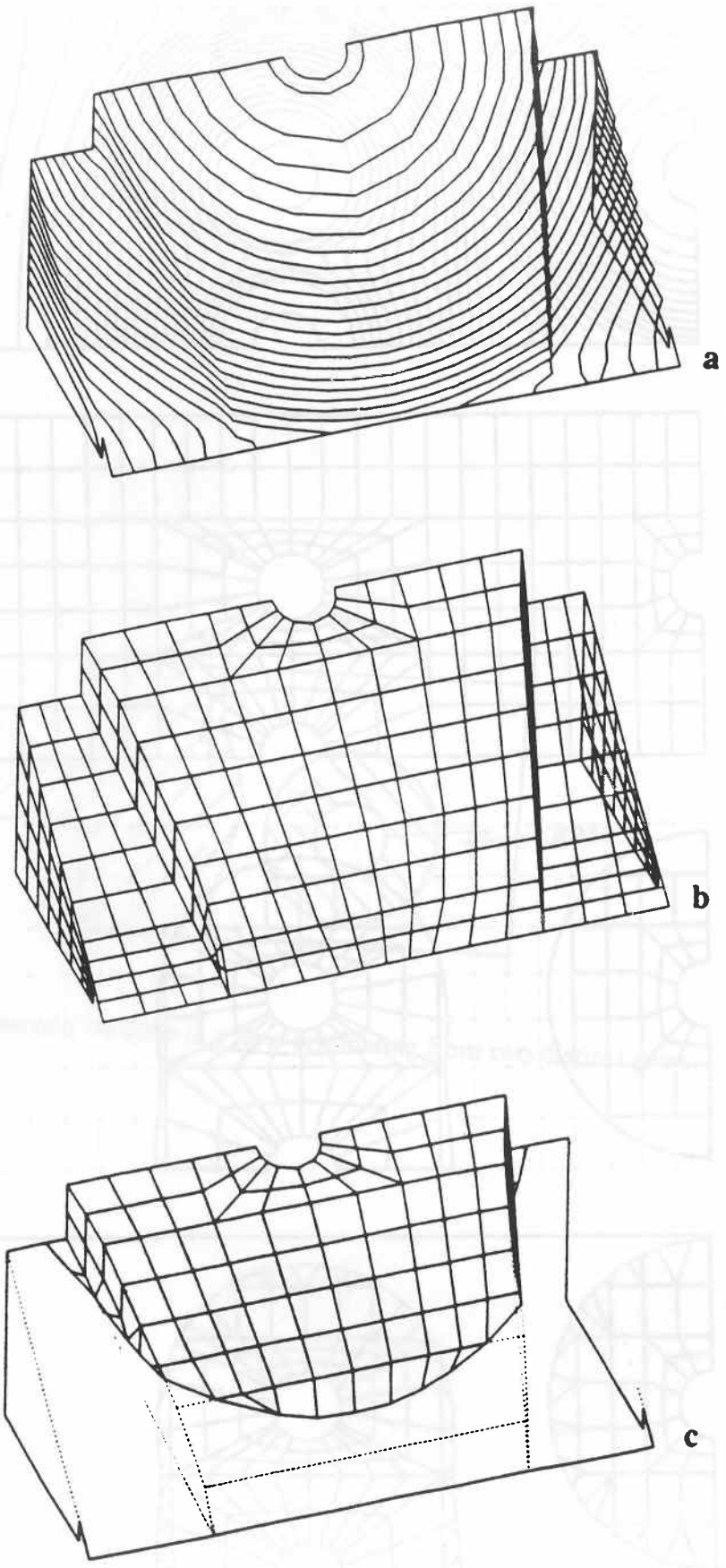

Fig.3. a. Successive flow fronts for the filling of a wind-breaker; b. initial finite element mesh; c. intermediate finite element mesh.

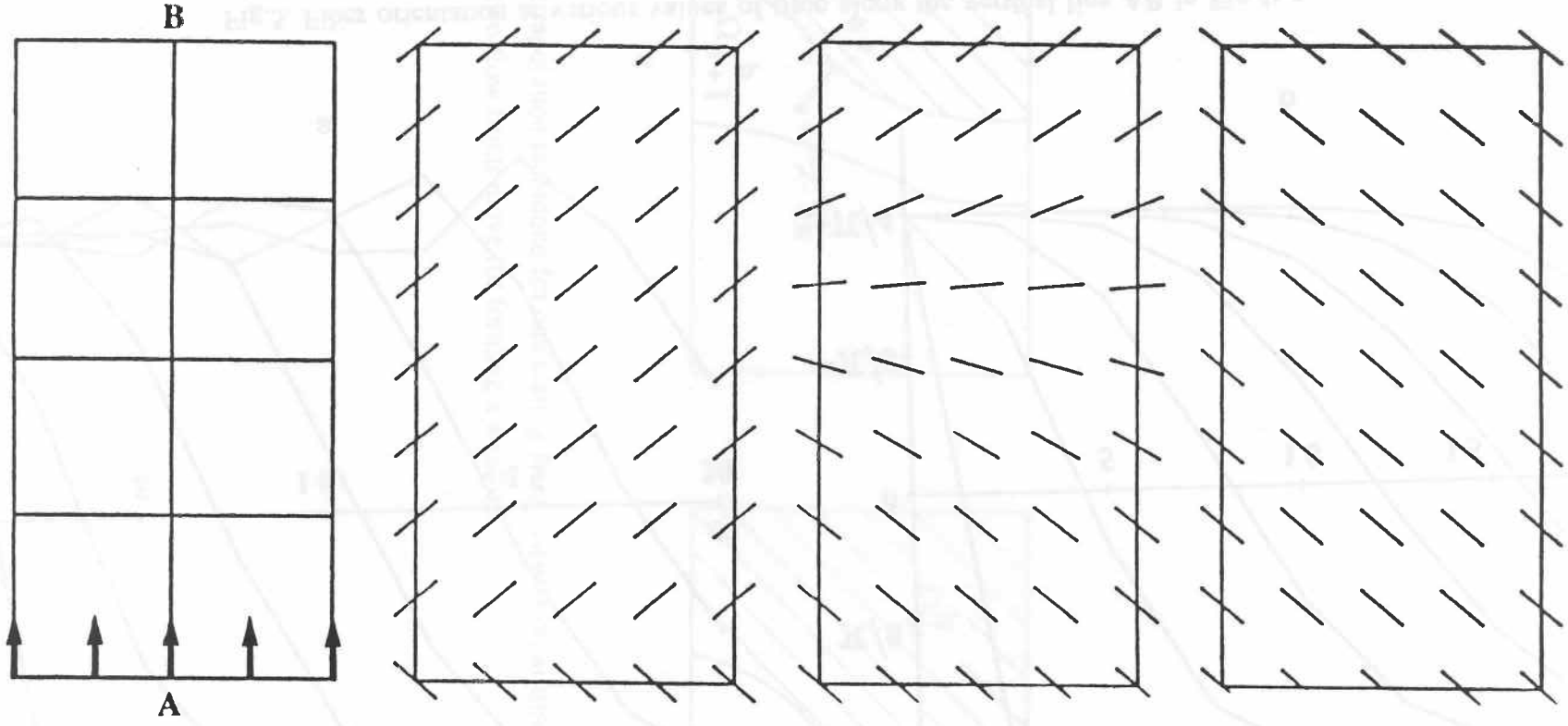

Fig.4. Uniform flow through a rectangular domain. A discontinuity in fiber orientation is propagated from the entry to the exit section.

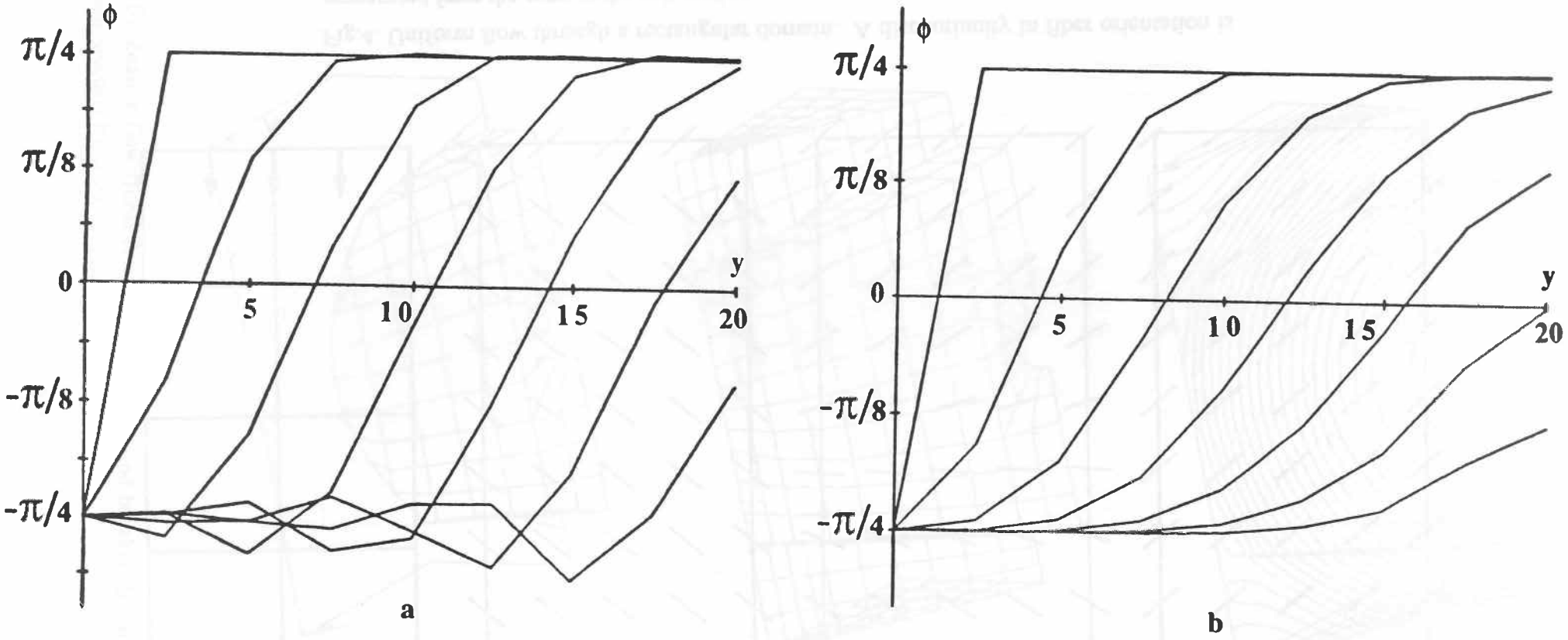

Fig.5. Fiber orientation at various values of time along the vertical line AB in Fig.4; a. Galerkin method; b. Streamline-upwind method.

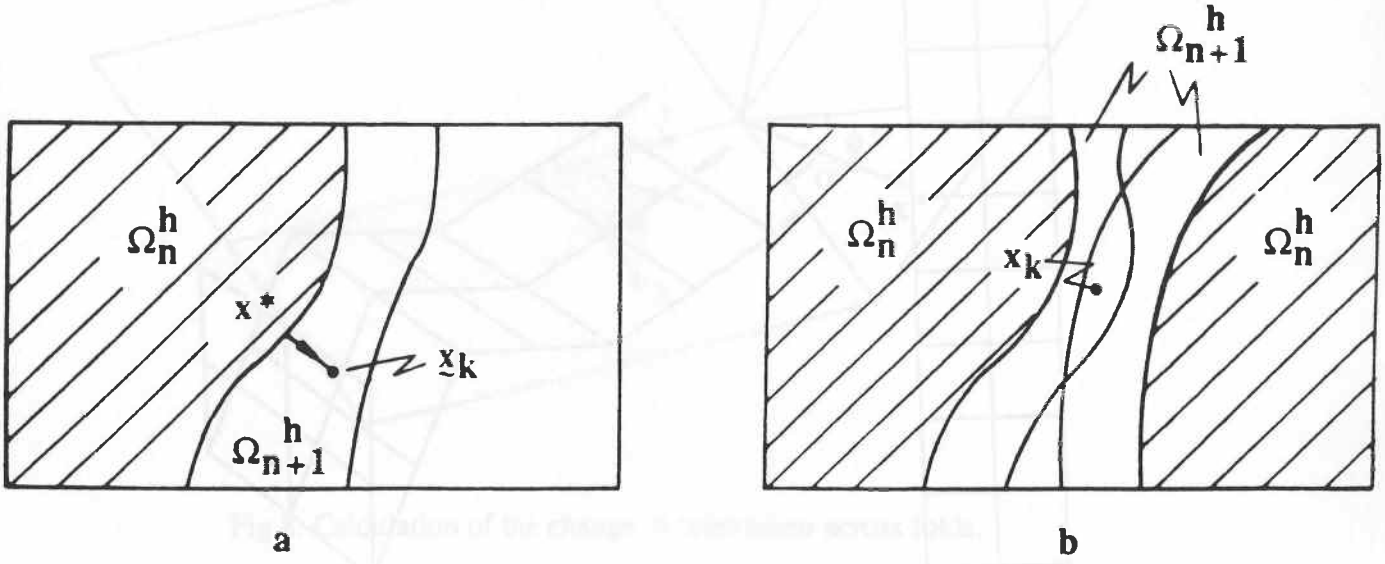

Fig.6. Extrapolation technique for calculating fiber orientation at time t_{n+1}; a. single flow front; b. two flow fronts move for forming a weldline.

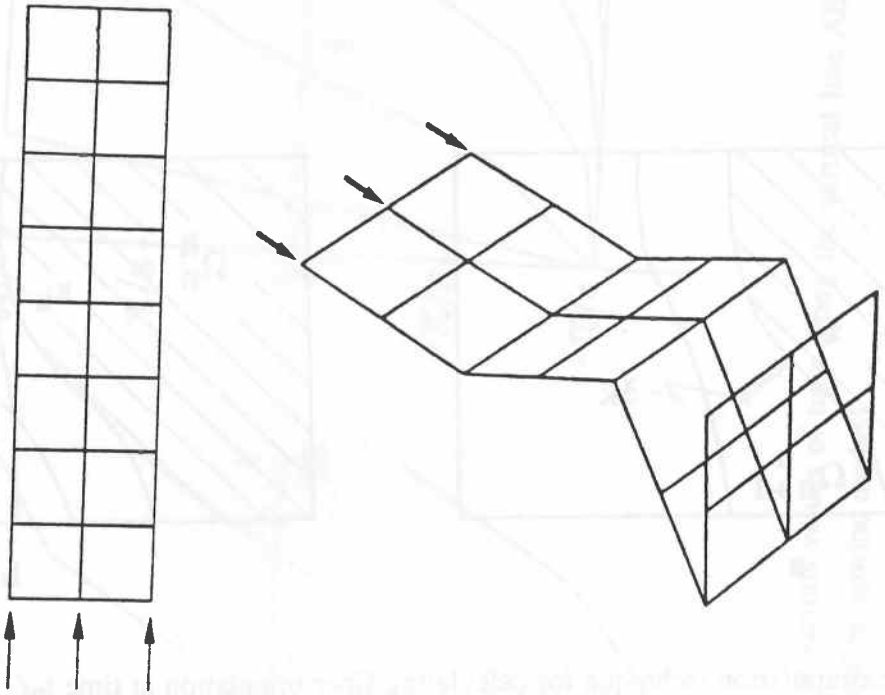

Fig.7. Flow in a plane mold and in a folded mold.

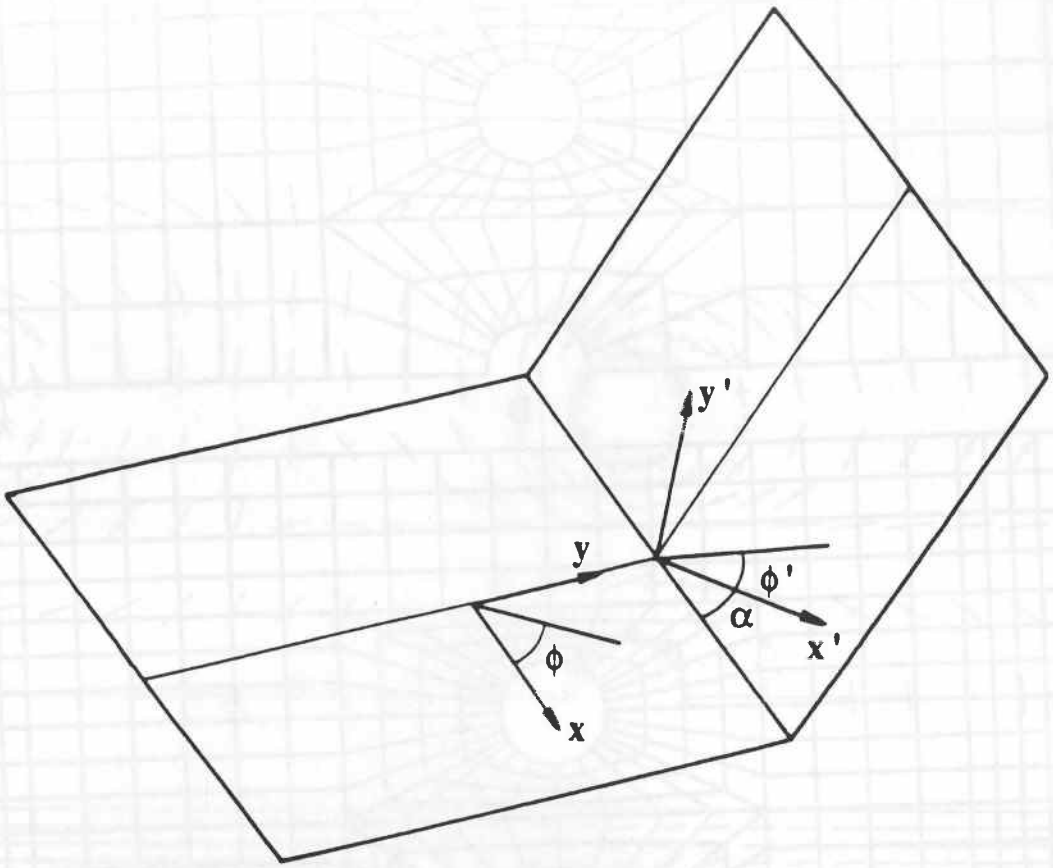

Fig.8. Calculation of the change of orientation across folds.

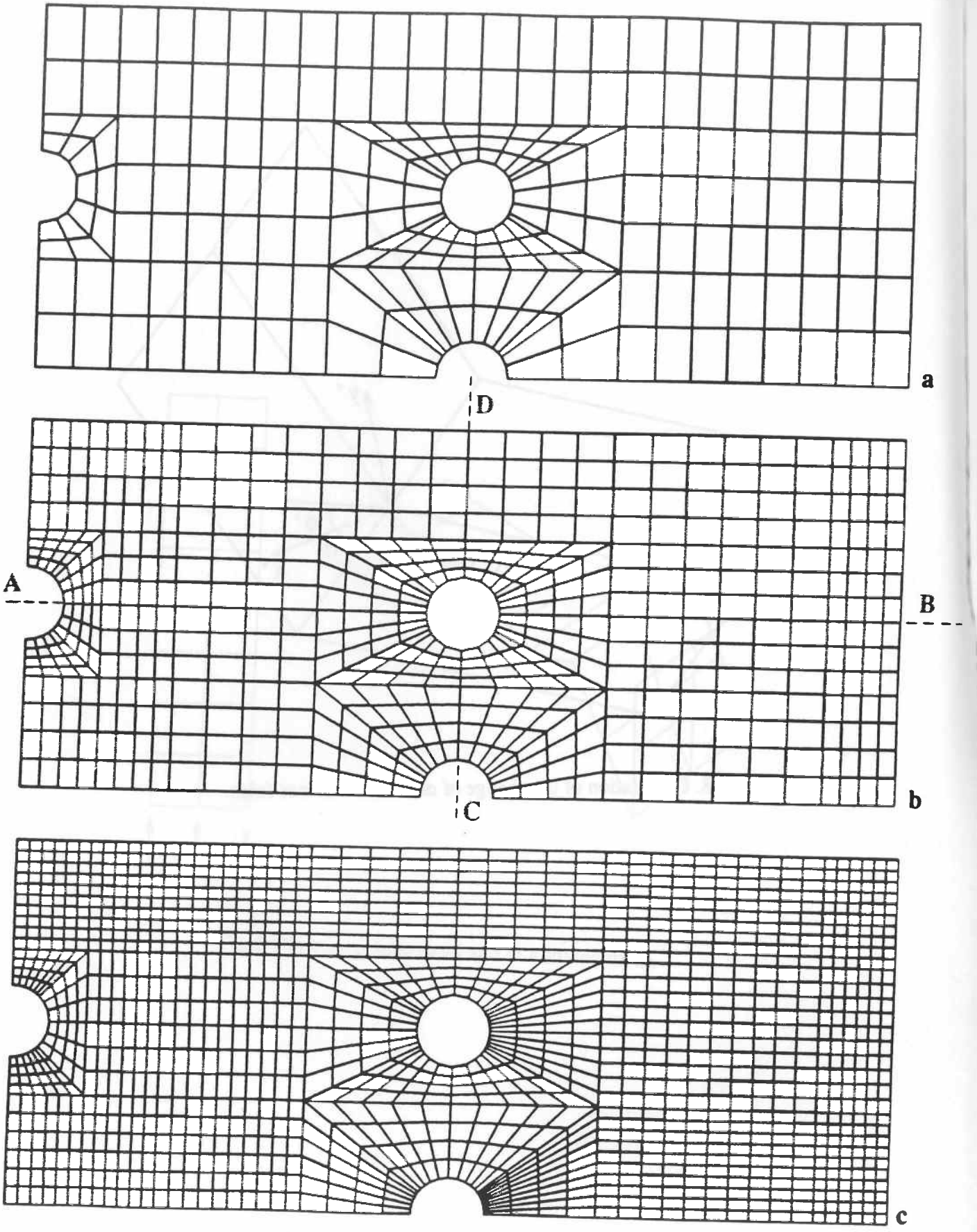

Fig.9. Three finite element meshes for the problem of Fig.2 containing respectively a. 276 elements, b. 622 elements, c. 1462 elements.

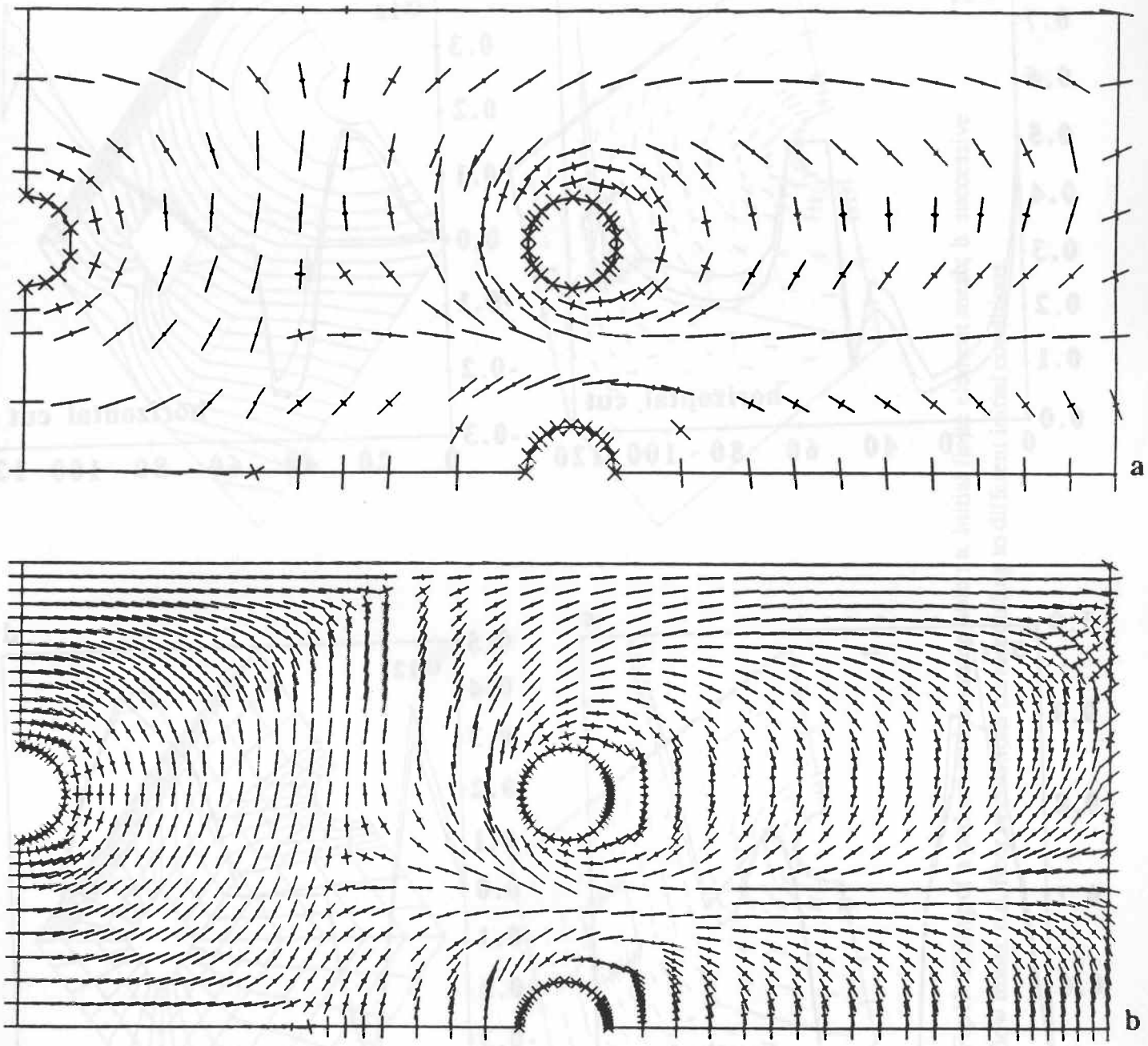

Fig. 10. Eigenvectors of the orientation tensor based on mesh a and mesh c of Fig.9.

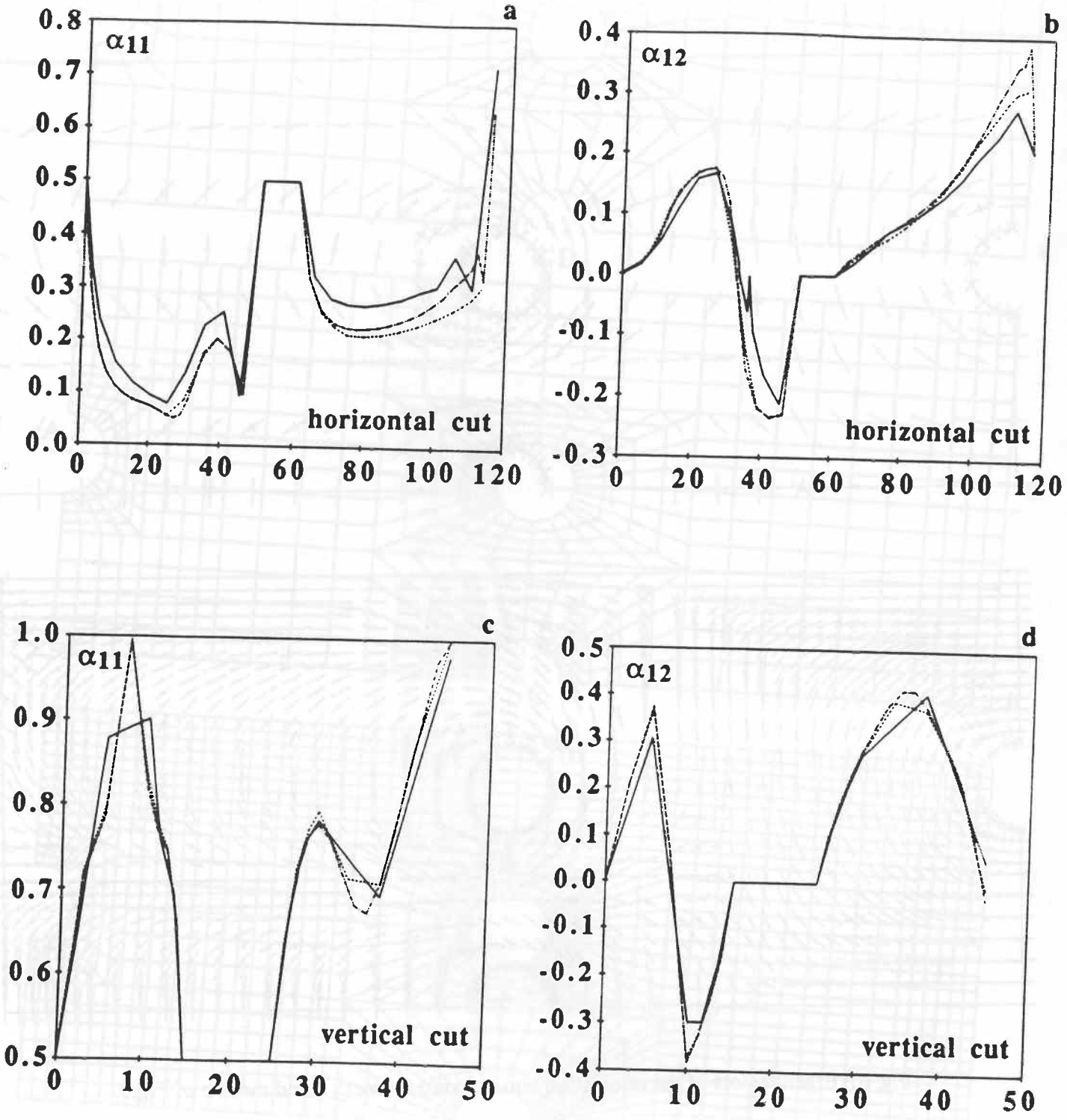

Fig.11. Components α_{11} and α_{12} of the orientation tensor plotted along the lines AB and CD shown in Fig.9 for finite element meshes a(—), b(---) and c (- — • —).

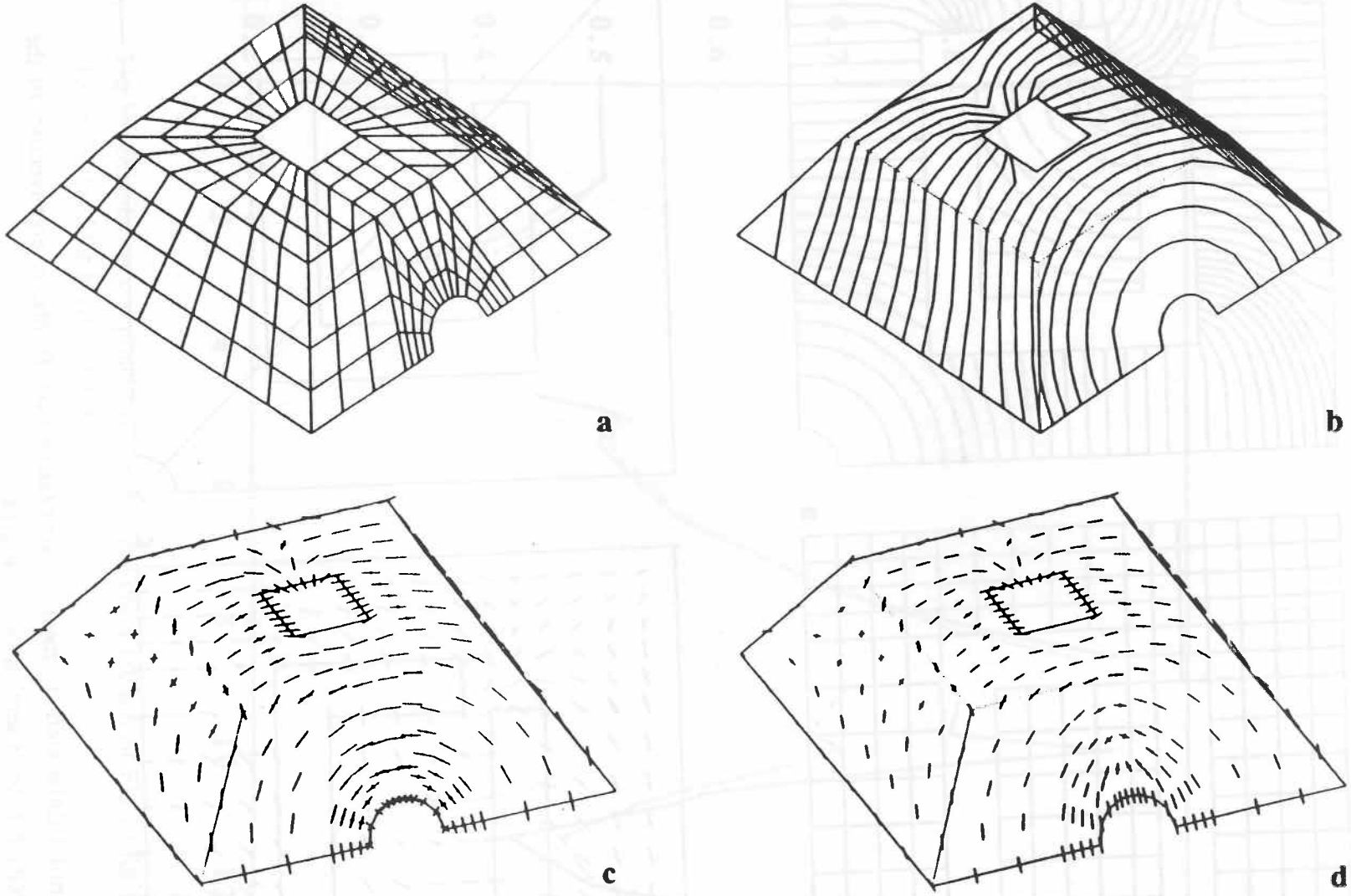

Fig.12. Filling of a podium with a square hole : a. initial finite element mesh; b. successive flow fronts; c.d, fiber orientations corresponding to different initial conditions.

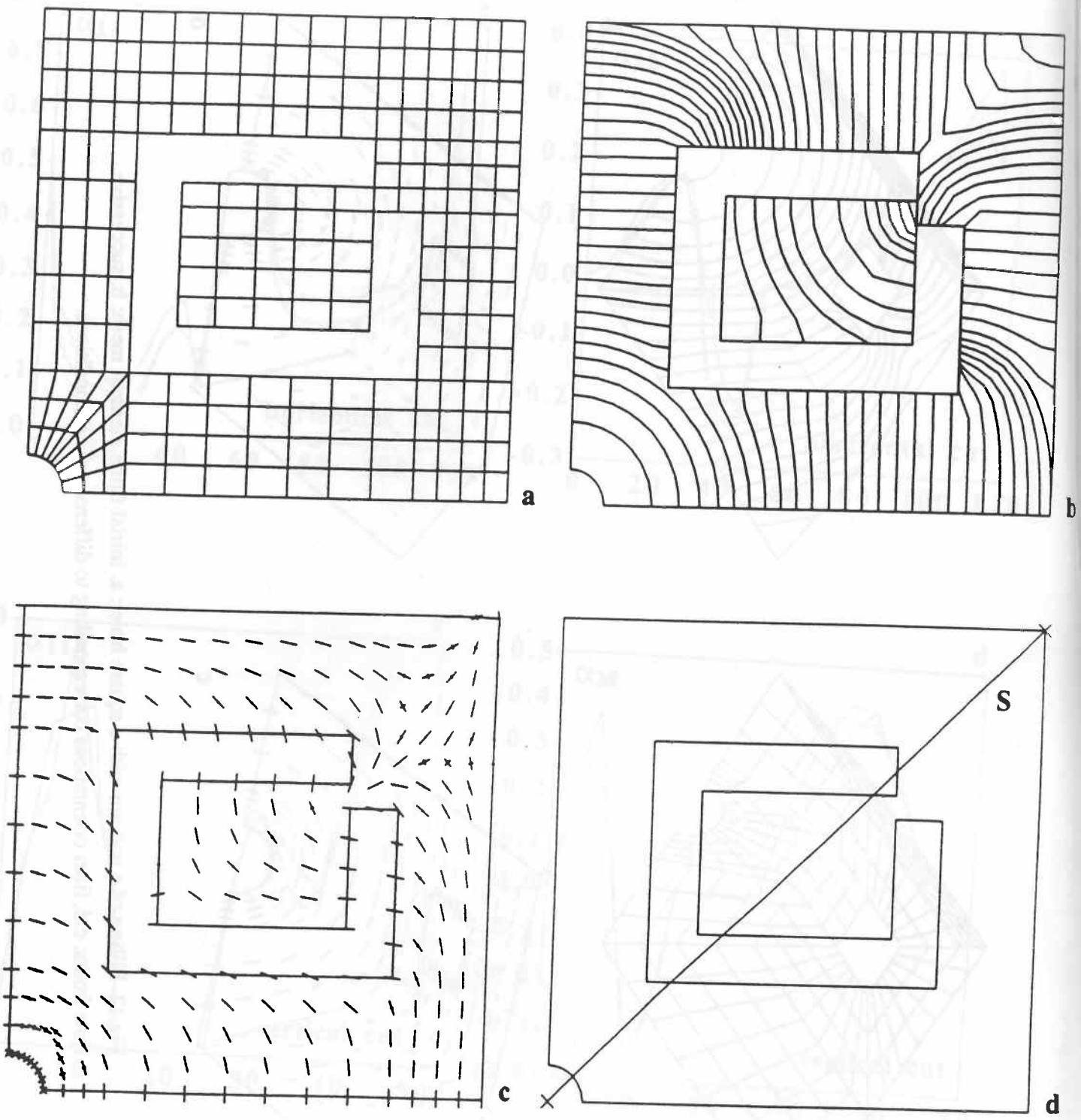

Fig.13. a. Initial finite element mesh; b. successive flow fronts; c. eigenvectors of the orientation tensor; c. cross section used in Fig.14.

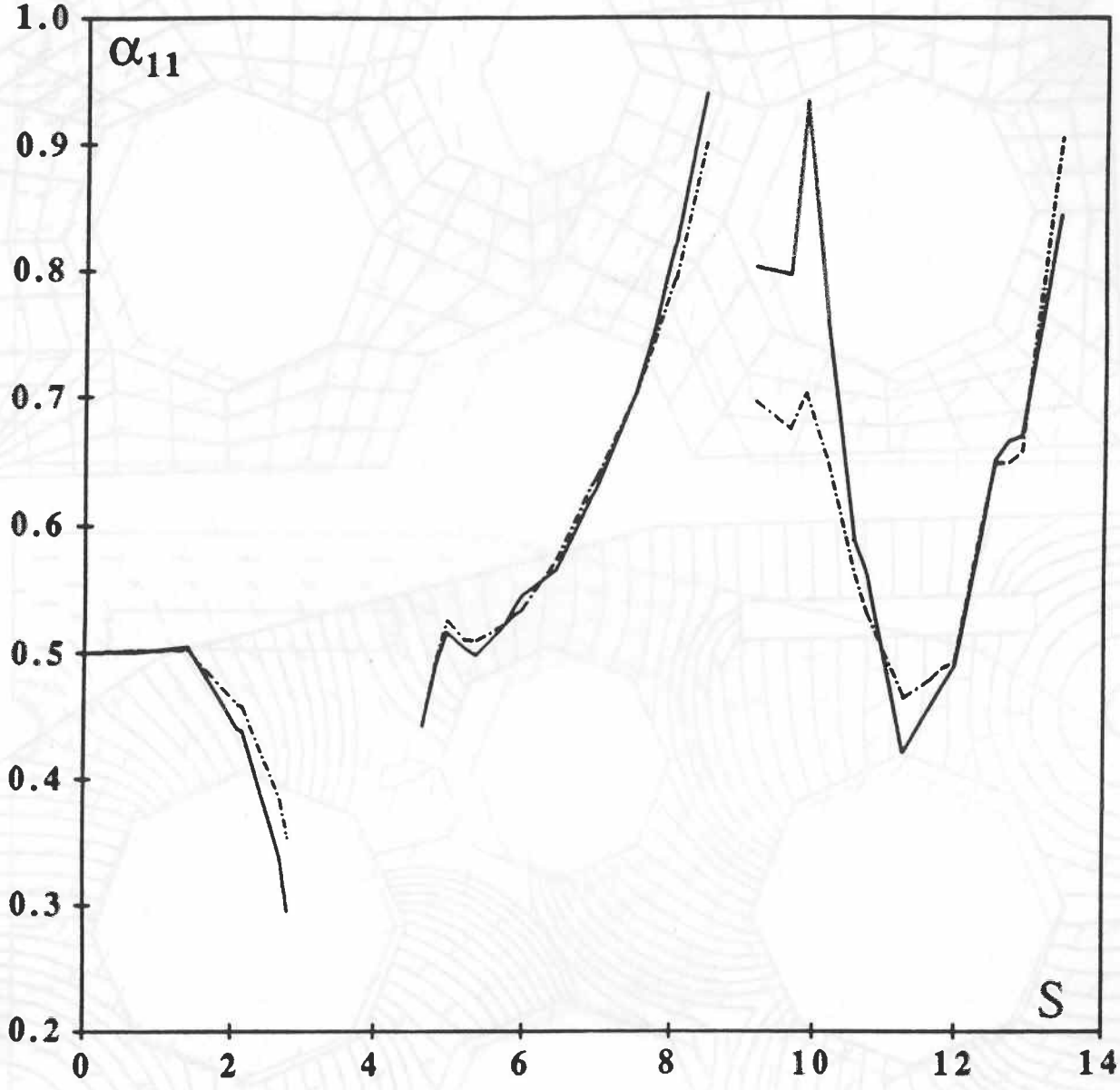

Fig.14. Orientation component α_{11} along the cross-section of Fig.13 for the quadratic closure (—) and the hybrid closure (- — • —).

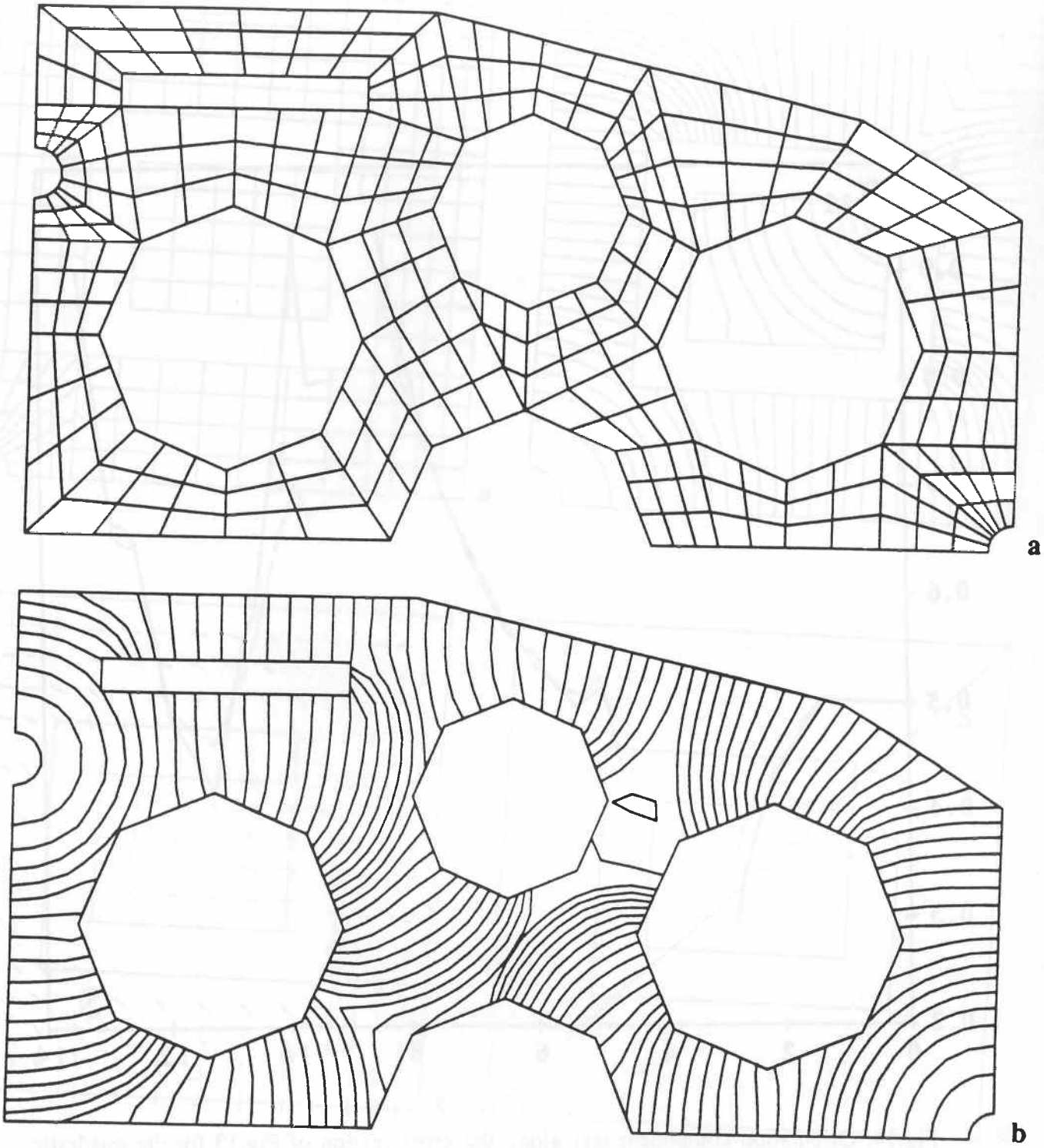

Fig.15. Filling of a dashboard with two gates : a. finite element mesh; b. successive flow fronts.

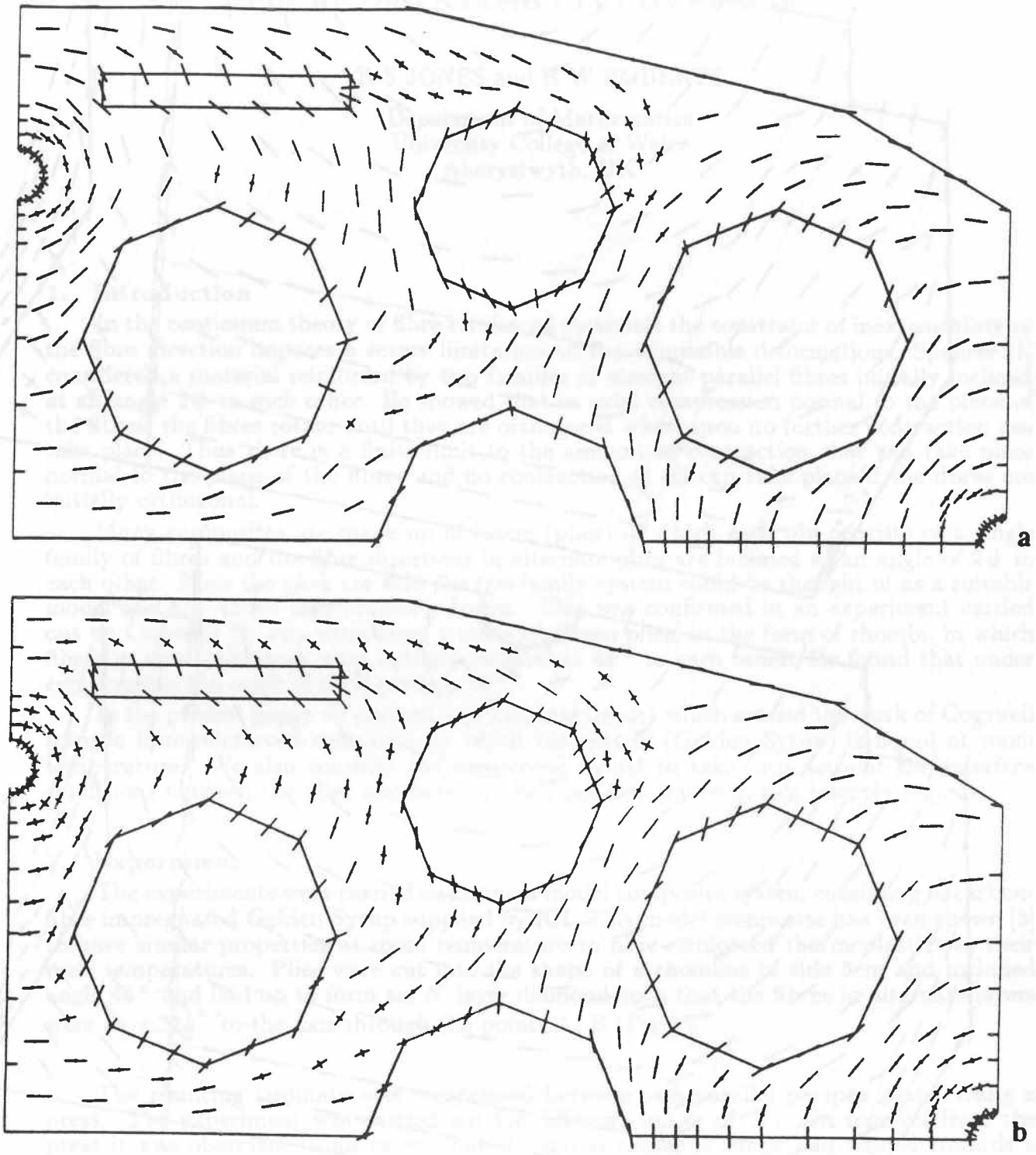

Fig.16. Fiber orientation distribution corresponding to the orientation tensor calculation (a) and Jeffery's law with three initial directions (b).

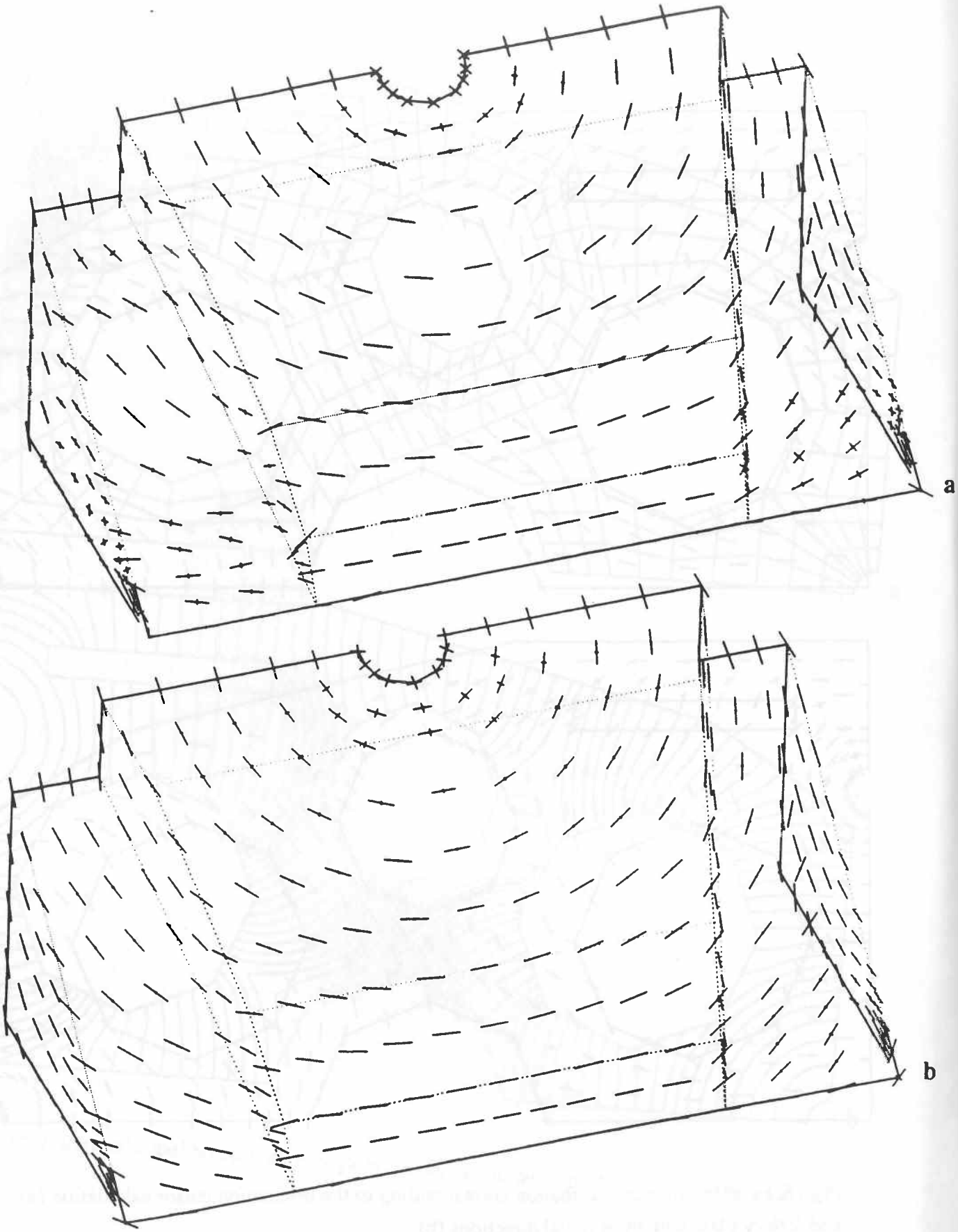

Fig.17. Fiber orientation in the wind-breaker of Fig.3 corresponding to the orientation tensor calculation (a) and Jeffery's law (b).